IOP Publishing Semiconductor Science and Technology
Semicond. Sci. Technol. 32 (2017) 085008 (7pp) https://doi.org/10.1088/1361-6641/aa74fe

Enhancement of P3HT organic photodiodes by the addition of a $GaSe_9$ alloy thin layer

M C Siqueira, A Hoff, C de Col, K D Machado, I A Hümmelgen and J P M Serbena[1]

Departamento de Física, Centro Politécnico, Universidade Federal do Paraná, 81531-990, Curitiba, Paraná, Brazil

E-mail: serbena@fisica.ufpr.br

Received 7 April 2017, revised 12 May 2017
Accepted for publication 25 May 2017
Published 12 July 2017

Abstract

We report on gallium–selenium alloy ($GaSe_9$) thin films simultaneously functioning as both blocking layer and active layer on poly(3-hexylthiophene-2, 5-diyl) (P3HT)-based organic photodiodes in order to enhance device performance. In addition to improved transport of the photogenerated charge carriers, $GaSe_9$ films also contribute to light absorption on a different wavelength interval than that of P3HT. Three different devices are compared: ITO/$GaSe_9$/Al, ITO/P3HT/Al and ITO/P3HT/$GaSe_9$/Al, with the last one presenting a lower dark current density (0.90 μA cm^{-2}), higher ON/OFF current ratio (61) and fastest response under AM 1.5 light irradiance. The observed responsivity is 7.3 mA W^{-1} and is almost linearly dependent on irradiance in the range 0.6–60 W m^{-2}. A maximum external quantum efficiency of 135% and specific detectivity of 16.7 $\times$ 10^{11} Jones at 390 nm incident light wavelength are obtained.

Supplementary material for this article is available online

Keywords: organic photodiode, hybrid device, selenium alloy

(Some figures may appear in colour only in the online journal)

Introduction

Photodiodes are among the most studied organic photodetectors due to their simplicity and ease of fabrication. They consist of an organic photoactive semiconductor in contact with two conducting electrodes, and are two-terminal devices either in planar or vertical architecture [1]. Planar geometry allows for direct light absorption, but the relatively large space between the electrodes reduces operation bandwidth, whereas vertical geometry enables faster collection of photoinduced charge and less charge accumulation [2]. At a reverse applied bias, the dark currents are usually lower, reducing device standby power consumption and increasing ON/OFF ratios. A possible way to further reduce dark current, thereby improving ON/OFF current ratio, relies on the insertion of a blocking layer near one or both electrodes. This approach is commonly used in organic light-emitting diodes [3] and solar cells [4] although, in these cases, the main objective is the prevention of exciton quenching near the electrodes. On photodiodes, a blocking layer may reduce hole injection from the cathode [5, 6]. Different materials and processes can be used for this purpose, either solution processed [7, 8], thermally sublimated [9, 10], fully spray coated [11] or ink-jet printed [12] photodiodes.

An interesting candidate for this objective is amorphous selenium (a-Se) and its alloys, due to their high work function (~6 eV), improved optical sensitivity and amorphous character [13]. Particularly in this case, the blocking layer would also participate in light absorption and photogeneration of charge carriers, because these composites are already used as active materials in, e. g., commercial photocopiers, highly sensitive television tubes based on high-gain avalanche rushing amorphous photoconductors [14] and highly sensitive biomedical x-ray imagers [15, 16]. By this method, in addition to the operation as a blocking layer, the semiconducting gallium–selenium alloy $GaSe_9$ would also advantageously operate as an active layer. Many optoelectronic properties and applications are under investigation by different research

[1] Author to whom any correspondence should be addressed.

groups [17–20], including integration with organic semiconductors as a promising way to enhance device characteristics, since a-Se/organic interfaces behave similarly to organic/organic interfaces in terms of energy level alignments and organic exciton dissociation [21].

In this work $GaSe_9$ is used to improve the characteristics of a poly(3-hexylthiophene-2, 5-diyl) (P3HT) organic photodiode. When constructed in a double layer, its high ionization energy prevents the injection of holes from the cathode and improves transport of the photogenerated charge carriers to the electrodes, reducing dark current and increasing photocurrent. In addition, it broadens the absorption range of the device.

Experimental

The devices were constructed using ITO-covered glass (LUMTEC, 15 $\Omega\,sq^{-1}$). The cleaning procedure consisted of ultrasonic bath (15 min in each case) in acetone, isopropyl alcohol and deionized water. The active layer consisted of P3HT only, $GaSe_9$ only or a P3HT/$GaSe_9$ bilayer. The regioregular P3HT (Sigma-Aldrich, regioregularity >90%) was used as received. The solution was prepared in toluene at a concentration of 7 mg l^{-1} using magnetic stirring at 60 °C. The P3HT layer was spin-coated onto the ITO layer at 1000 rpm for 10 s, and 2000 rpm for 30 s, to obtain a 40 nm thick layer with ~6 nm roughness. It was then thermally annealed at 100 °C in a vacuum for 30 min. The $GaSe_9$ alloy was prepared by mechanical alloying following a procedure reported in [22] and deposited in the form of 20 nm thick film using thermal evaporation at base pressure of 10^{-6} Torr. In the sequence, approximately 100 nm of Al was deposited by vacuum thermal evaporation on top of the active layer, at a base pressure of 10^{-6} Torr, obtaining the final structure ITO/P3HT/Al, ITO/$GaSe_9$/Al or ITO/P3HT/$GaSe_9$/Al. The device active area, controlled through shadow masks, was 3 mm^2. All devices were characterized in air. Their stability allowed measurements on the same or the next day of fabrication, under low stress conditions.

Absorption measurements were carried out using a Shimadzu UV 2401 PC UV–vis spectrophotometer. Electrical measurements were carried out in darkness and under AM 1.5 light using a Keithley 6487 picoammeter/voltage source or a Keithley 2400 source/measure unit and a Thermo-Oriel solar simulator. Irradiance was varied using neutral density filters from Thorlabs Inc. Atomic force microscopy (AFM) images were recorded with a Shimadzu SPM-9500 J3 microscopy in dynamic mode. Thicknesses were measured using a Bruker DektakXT stylus profiler.

Results and discussion

Figure 1 presents AFM images of the active layer thin film surfaces P3HT (figure 1(a)) and P3HT/$GaSe_9$ (figure 1(b)) over the ITO substrate. It can be observed that the morphology of the P3HT film is formed by sharper peaks and deeper valleys than the $GaSe_9$ film over P3HT, as quantitatively measured by roughness: 1.31 nm rms for the ITO/P3HT film and 0.66 nm rms for the ITO/P3HT/$GaSe_9$ film. This indicates that the deposition of the inorganic semiconductor alloy $GaSe_9$ smooths the active layer surface prior to deposition of the metallic electrode, a characteristic that can reduce the probability of short circuit due to pinholes or metallic diffusion into the semiconductor. The interface between P3HT and $GaSe_9$ in the bilayer device is expected to follow the shape of the P3HT surface profile, with the $GaSe_9$ material penetrating the valleys and surpassing the peaks. This rougher interface will increase the contact area between the materials, a characteristic that favors exciton dissociation and promotes shorter channels for the charge carriers to cross the semiconductors and reach the electrodes.

Figure 2(a) shows the structure of the ITO/P3HT/$GaSe_9$/Al photodiodes. The ITO/$GaSe_9$/Al and ITO/P3HT/Al devices have a similar structure, except for the absence of one of the layers. Figure 2(b) presents a flat band energy diagram of the isolated materials used in this work, with respective work functions or frontier energy levels of ITO [23], $GaSe_9$ [24], P3HT [25] and Al [26].

Both materials are photosensitive, as observed on figures 3(a) and (b) which show the current versus voltage measurements of the ITO/P3HT/Al and ITO/$GaSe_9$/Al devices in darkness and under 60 W m^{-2} AM 1.5 light irradiance through the ITO electrode; this means that $GaSe_9$ also contributes to photogeneration of charge carriers in the bilayer device. Both devices have single charge carrier dominated transport, as observed by their symmetric curves. The light/dark for both materials is higher at negative bias. Although $GaSe_9$ thin film has higher photocurrent than P3HT at the same voltage, its dark current is also higher, which degrades the device ON/OFF ratio. However, if both materials are combined in an active bilayer, ITO/P3HT/$GaSe_9$/Al, the device photoresponse is considerably improved, as shown in figure 3(c). The origin of the illuminated S-shaped current–voltage curve observed on the bilayer device can be due to different processes, but is usually associated with an enhanced charge recombination at the donor/acceptor interface [27] or to a non-ideal semiconductor/metallic cathode interface [28, 29], which leads to a potential barrier for charge collection [30]. Table 1 summarizes the results for the three devices.

Even though a higher photocurrent is observed at positive voltage, at negative voltage there is a strong decrease in dark current, allowing an increased ON/OFF ratio at the same voltage when compared to the other devices. In darkness, it is expected that only charge carriers injected from the electrodes contribute to the total current. From the view of the band energy diagram presented in figure 2, it is expected that, in darkness at positive bias (figure 4(a)), although there is a small energy barrier for charge injection from the electrodes, an internal barrier for both electrons and holes exists due to the difference in HOMO and LUMO levels of both materials, which may contribute to the increase in recombination current. In darkness at negative bias (figure 4(b)), the total current is lower because of the high energy barrier for injection

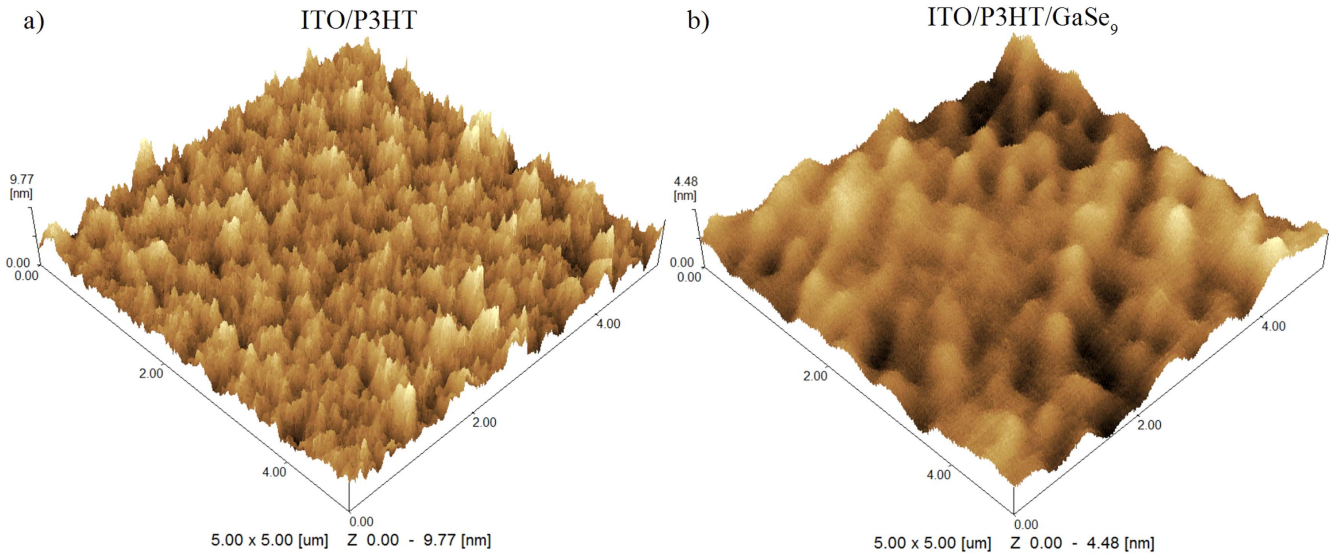

Figure 1. AFM images of (a) ITO/P3HT and (b) ITO/P3HT/$GaSe_9$ surface thin films.

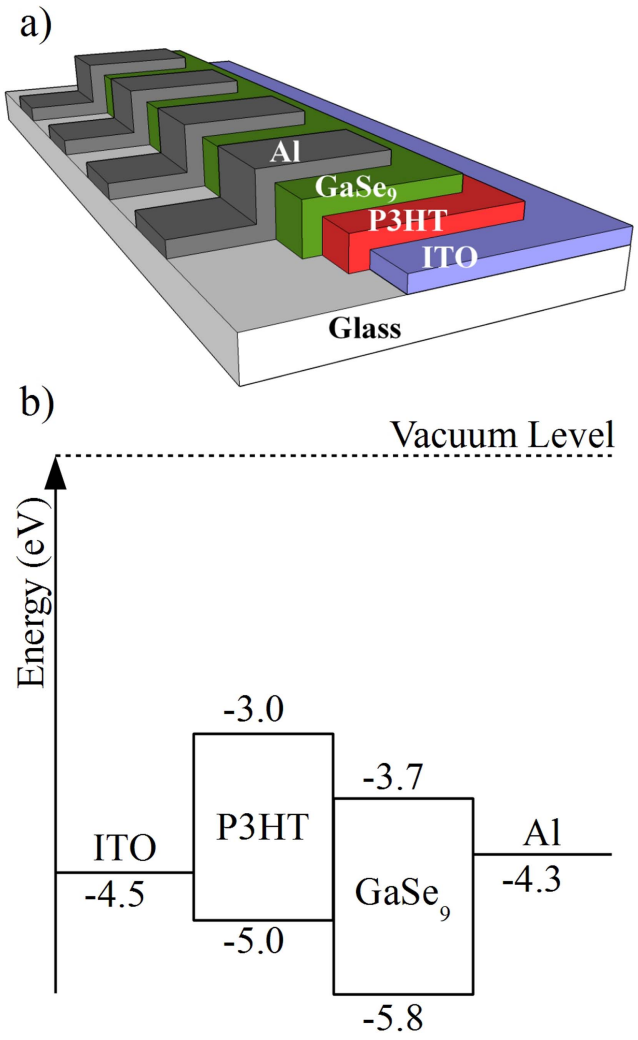

Figure 2. (a) Sandwich structure in which the devices were constructed. The electrodes are ITO and Al. The active layer is P3HT only, $GaSe_9$ only or a P3HT/$GaSe_9$ bilayer. (b) Flat band energy level diagram of the isolated materials involved in this work.

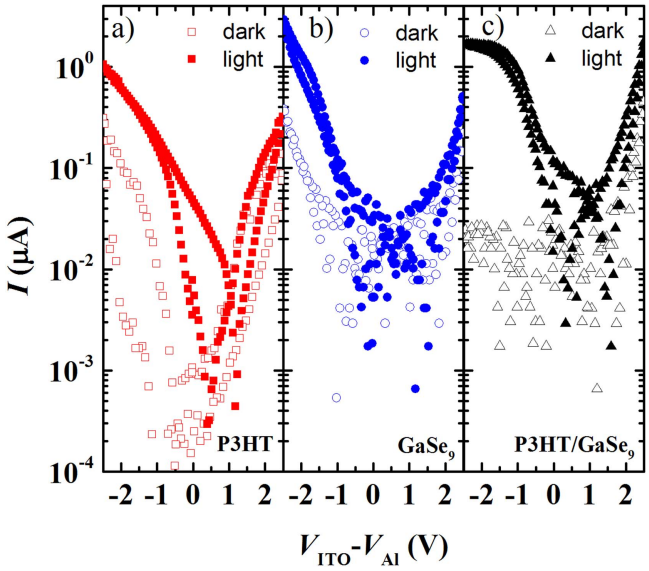

Figure 3. Current versus voltage curves in darkness and under white light illumination of 60 W m^{-2} of (a) ITO/P3HT/Al, (b) ITO/$GaSe_9$/Al, (c) ITO/P3HT/$GaSe_9$/Al devices. The illumination occurs through the ITO side.

Table 1. Dark current densities and ON/OFF ratios for ITO/P3HT/Al, ITO/$GaSe_9$/Al and ITO/P3HT/$GaSe_9$/Al phodetectors at 2 V negative bias under AM 1.5 light irradiance.

Active iayer	P3HT	$GaSe_9$	P3HT/$GaSe_9$
J_{DARK} (μA cm^{-2})	4 ± 1	4 ± 1	0.8 ± 0.2
ON/OFF ratio	5.6 ± 0.9	7.2 ± 0.9	63. 8 ± 0.6

of charge carriers from the electrodes, which leads to a low dark current. Under light incidence, it is expected that both injected and photogenerated charge carriers contribute to the total current. In light at positive bias (figure 4(c)), a significant increase on current values is not observed, indicating that,

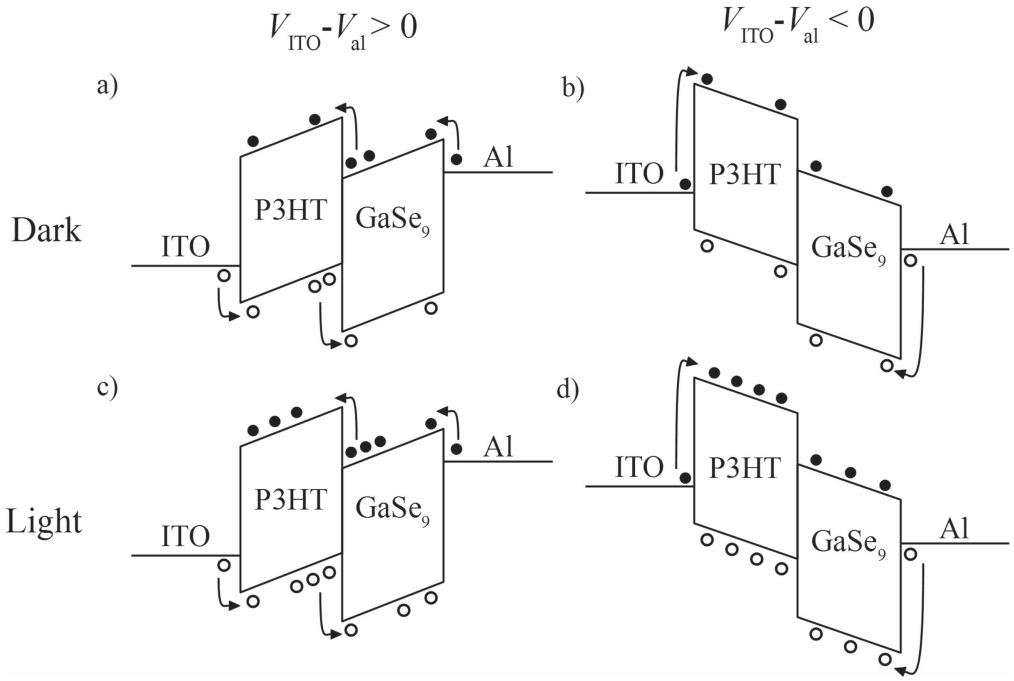

Figure 4. Illustrative collection of charge carriers: both photogenerated and injected by the electrodes at (a) dark positive applied bias, (b) dark negative applied bias, (c) light incidence positive applied bias and (d) light incidence negative applied bias. Holes are open circles and electrons are solid circles. Arrows indicate the presence of an energy barrier due to differences in band energy levels.

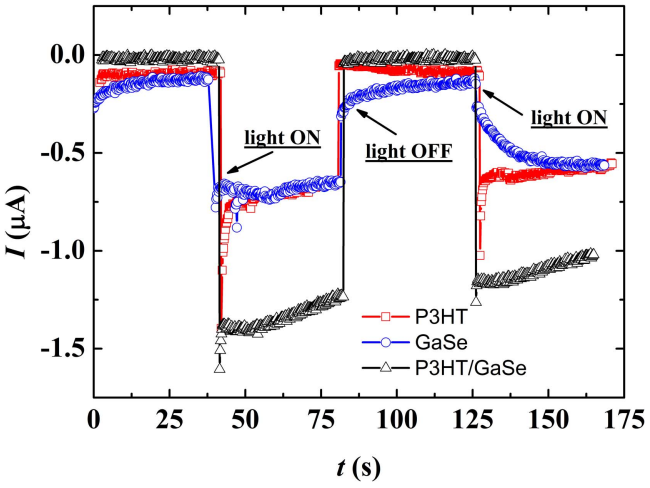

Figure 5. Time response of the three devices in darkness and under 60 W m^{-2} AM 1.5 light irradiance. The device area is 3 mm^2. Sampling rate: 10 points per second.

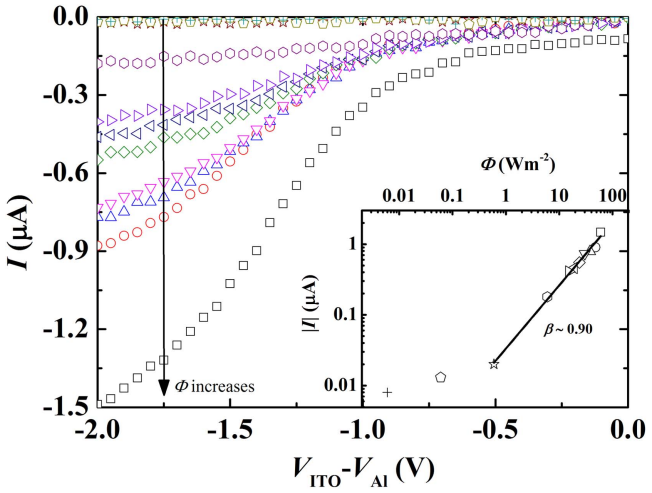

Figure 6. Current versus voltage curves of the ITO/P3HT/$GaSe_9$/Al device under different white light irradiance. Inset: current versus irradiance linear behavior of the device at 2 V reverse bias. Dark current corresponds to the + symbol. The device area is 3 mm^2. β is the slope of the log-log fit.

although there is a contribution from photogenerated charge carriers, only the electrons photogenerated in the P3HT and the holes photogenerated in the $GaSe_9$ layers are collected at the ITO and Al electrodes, respectively. The holes photogenerated in the P3HT and the electrons photogenerated in the $GaSe_9$ are blocked at the interface between both materials, which may increase the recombination current. In contrast, in light at negative bias (figure 4(d)), the photogenerated electrons and holes generated in both materials are collected by the Al and ITO electrodes, respectively, since an internal energy barrier is absent, leading to a significant increase in measured total current.

Figure 5 presents the time dependence of the photoresponse of the three devices at an applied voltage of −2 V and 60 W m^{-2} AM 1.5 light irradiance. It can be observed that the bilayer device has an increased photocurrent and a lower OFF current than both monolayer devices. Although all of them present fast response times, which could not be measured by the setup used, the photocurrents achieve steady-state values faster in the bilayer device in less than 0.1 s. This indicates that $GaSe_9$ not only helps to absorb light, but also improves charge separation and transport in the active layer,

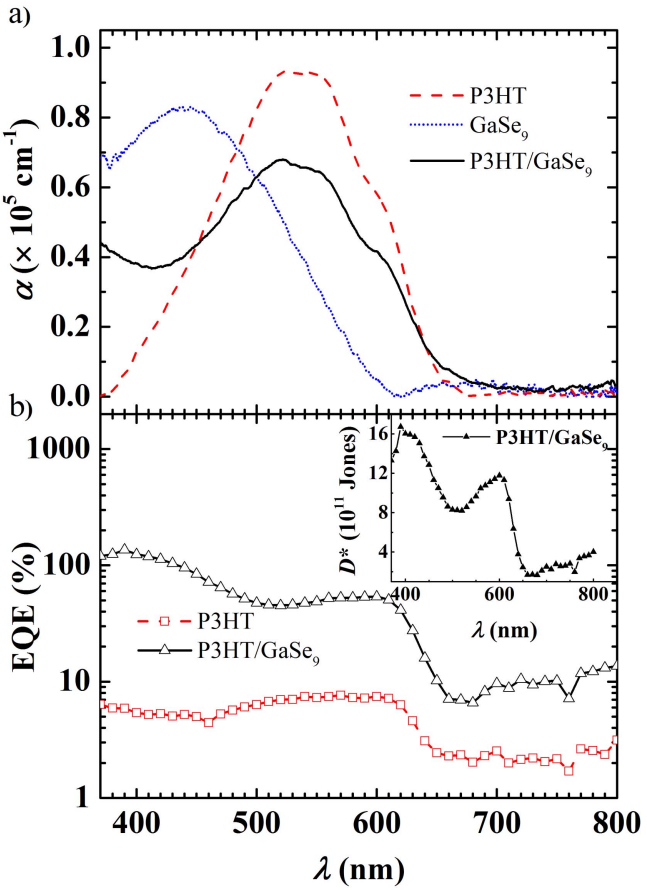

Figure 7. (a) Absorption coefficient of P3HT, $GaSe_9$ and P3HT/$GaSe_9$ films over glass substrates in the visible range. (b) External quantum efficiency (EQE) in the visible range of ITO/active layer/Al photodiodes, where the active layer is P3HT or P3HT/$GaSe_9$. Inset: specific detectivity as a function of wavelength for the ITO/P3HT/$GaSe_9$/Al device.

decreasing charge accumulation, possibly due to internal recombination at the internal P3HT/$GaSe_9$ interface.

One of the key parameters in characterizing a photodiode is its responsivity R, which is defined as the ratio of photogenerated current and irradiance. Figure 6 showss the photocurrent as a function of voltage for different AM 1.5 light irradiances. The onset is approximately 0.8 V for all curves, the stronger response occurring at 2 V reverse bias and higher irradiance, 60 W m^{-2}. It is easily observable that the photocurrent increases with irradiance and that this increase is almost linear, giving rise to an almost constant average responsivity, as presented in the inset of figure 6. By considering the device active area, the responsivity of this hybrid organic/inorganic device can be estimated as 7.3 mA W^{-1}, still below values reported in the literature for organic photodetectors [1] or inorganic selenium-based devices [17, 31, 32].

In a bilayer broad range photodetector, overlap of the materials' absorption spectra is desired mainly at the edges of the absorption curves of the isolated materials, instead of at the peaks. Figure 7(a) presents the absorption coefficient of the materials used in this work, deposited over glass substrates. Layer thicknesses are 40 nm for P3HT and 20 nm for $GaSe_9$. It is observed that the active bilayer P3HT/$GaSe_9$ has a broader absorption range than the active single layers P3HT and $GaSe_9$, the former being responsible for longer wavelength absorption and the latter for shorter wavelength absorption. The absorption peak of P3HT/$GaSe_9$ coincides with that of P3HT (525 nm), indicating that it has a more efficient absorption process than the $GaSe_9$ layer. This is expected if one compares, for example, the maximum absorption coefficients of the two materials: 0.94 × 10^5 cm^{-1} (P3HT) and 0.82 × 10^4 cm^{-1} ($GaSe_9$). However, apart from efficient light absorption, efficient pair dissociation and collection of charges at the electrodes is also required. From this viewpoint, $GaSe_9$ plays a key role due to its low valence band energy level.

Figure 7(b) presents the external quantum efficiency (EQE) as a function of incident light wavelength for the studied devices ITO/P3HT/Al and ITO/P3HT/$GaSe_9$/Al. The result for the ITO/$GaSe_9$/Al device is absent because it degrades during measurement, making it impossible to analyze. Regarding thestability of the ITO/$GaSe_9$/Al device, it is important to note that the $GaSe_9$ film thickness is the same in both the ITO/$GaSe_9$/Al and ITO/P3HT/$GaSe_9$/Al devices. In this way, when applying the same voltage, the electric field to which the active layer, and consequently the $GaSe_9$ layer, is subjected is much higher in the former than in the latter, meaning also a higher electrical stress. The diffusion of atoms from the electrodes into the active layer is a process known to occur in conjugated polymers. For example, Gallardo *et al* [33] reported the diffusion of indium and aluminum into polydiallyl-dimethyl-ammonium when submitted to high electric fields. Due to the similarities between amorphous selenium alloys and conjugated polymers, we believe this to be the main cause of the ITO/$GaSe_9$/Al device instability. From this viewpoint, ITO/P3HT/$GaSe_9$/Al devices are more stable because of the lower internal electric field and thicker active layer, which may inhibit the formation of a percolation path formed from diffused electrode atoms. In addition, AFM images reveal that the interface $GaSe_9$/Al is free of spikes, which would typically increase the local electric field. Finally, this instability is probably not associated with a photophysical or photochemical process because it is observed even in the absence of light, although light may favor its occurrence. The EQE is a parameter used to quantify the photogenerated charge carriers per single incident photon. It can be defined as [34]:

$$\mathrm{EQE} = \frac{hc}{q\lambda}R \tag{1}$$

where c is the speed of light. It is observed that there is a tendency for the EQE spectrum to follow the absorption spectrum for each active layer, reaching its maximum of 135% at 390 nm for the bilayer device. Their amplitudes indicate that the $GaSe_9$ alloy also contributes to the observed photocurrent under AM 1.5 light irradiance. In particularly, for the P3HT/$GaSe_9$ active bilayer, there is an increase at shorter wavelengths, the region corresponding to absorption mainly due to $GaSe_9$. Usually, EQE values higher than 100% are associated with photomultiplication [35], and avalanche

production of charge carriers may possibly have a major role, which is well known and documented to occur on amorphous Se films under high electric fields [36]. However, this hypothesis applied to our devices needs further investigation before confirmation. At longer wavelengths, 650 nm to 800 nm, a higher EQE is observed for the P3HT/$GaSe_9$-based device than for the P3HT-based device, although both materials show negligible absorption at this interval. Considering the low absorption coefficient of these materials at this interval, it is expected that most of the incident light is not absorbed by the P3HT/$GaSe_9$ bilayer, being transmitted through it and reaching the $GaSe_9$/Al interface. As the energy of the photons is equal to or higher than the energy barrier height for hole injection from Al into $GaSe_9$, approximately 1.5 eV, the photocurrent signal measured at this interval can be attributed to internal photoemission of charge carriers from the electrode into the semiconductor layer. This process allows the absorption of photons with energies lower than the semiconductor bandgap, increasing its detection bandwidth, and is usually employed in the fabrication of infrared Schottky photodetectors [37–39]. In addition, it is likely that the insertion of the $GaSe_9$ layer severely diminishes quenching of the photogenerated excitons near the metallic electrode, a process that can decrease the device quality, because it drives away P3HT from the electrode interface. It is reported that the organic/metallic interfaces show high non-radiative recombination rates, the quenching zone being of the order of 10 nm, lower than the $GaSe_9$ layer thickness, [40, 41].

The inset of figure 7(b) presents the specific detectivity as a function of incident light wavelength for the ITO/P3HT/$GaSe_9$/Al device, as calculated from [42]:

$$D^* = \frac{RA^{1/2}}{(2qI_{\text{dark}})^{1/2}} \tag{2}$$

where A is the active device area and I_{dark} is dark current, and assuming shot noise as the major contributor to the total noise. A maximum of 16.7×10^{11} Jones is obtained at 390 nm. The specific detectivity is higher at wavelengths near the absorption regions of P3HT and $GaSe_9$, indicating once more that $GaSe_9$ contributes to photon absorption and charge generation in the bilayer device.

Conclusions

We demonstrated the enhancement in the performance of a P3HT-based organic photodetector by the introduction of a thin inorganic layer of $GaSe_9$ alloy. AFM images indicate that the surface of the P3HT thin film is rougher than that of the $GaSe_9$ thin film, which indicates that the interface P3HT/$GaSe_9$ has a higher surface area than the interface $GaSe_9$/Al. The improvements are a broader absorption spectrum, higher ON/OFF ratio, lower dark current, linear responsivity on incident AM 1.5 light irradiance, and higher EQE at different incident light wavelengths. Due to its energy levels, the $GaSe_9$ layer is able to collect photogenerated electrons form P3HT and inject photogenerated holes into it, increasing the measured photocurrent. The chalcogenide alloy is not only responsible for blocking undesired charge carriers but also contributes to the absorption of incident light, and generation and collection of photocurrent. Finally, the $GaSe_9$ layer can be considered as both a blocking layer and an active layer in these devices.

Acknowledgments

The authors would like to thank the Brazilian agencies CNPq and CAPES for financial support.

ORCID

J P M Serbena https://orcid.org/0000-0003-4286-5064

References

[1] Baeg K J, Binda M, Natali D, Caironi M and Noh Y Y 2013 *Adv. Mater.* **25** 4267–95
[2] Agostinelli T, Caironi M, Natali D, Sampietro M, Biagioni P, Finazzi M and Duo L 2007 *J. Appl. Phys.* **101** 114504
[3] Adamovich V I, Cordero S R, Djurovich P I, Tamayo A, Thompson M E, B D'Andrade W and Forrest S R 2003 *Org. Electron.* **4** 77–87
[4] Po R, Carbonera C, Bernardi A and Camaioni N 2011 *Energy Environ. Sci.* **4** 285–310
[5] Valouch S, Hönes C, Kettlitz S W, Christ N, Do H, Klein M F G, Kalt H, Colsmann A and Lemmer U 2012 *Org. Electron.* **13** 2727–32
[6] Gong X, Tong M H, Park S H, Liu M, Jen A and Heeger A J 2010 *Sensors* **10** 6488
[7] Keivanidis P E, Khong S-H, Ho P K H, Greenham N C and Friend R H 2009 *Appl. Phys. Lett.* **94** 173303
[8] Cheung C H, Kim D Y, Subbiah J, Amb C M, Reynolds J R and So F 2014 *IEEE T. Electron Dev.* **61** 3852–7
[9] Leem D S, Lee K H, Park K B, Lim S J, Kim K S, Jin Y W and Lee S 2013 *Appl. Phys. Lett.* **103** 043305
[10] Hammond W T, Mudrick J P and Xue J 2014 *J. App. Phys.* **116** 214501
[11] Tedde S F, Kern J, Sterzl T, Fürst J, Lugli P and Hayden O 2009 *Nano Lett.* **9** 980–3
[12] Lilliu S, Boeberl M, Sramek M, Tedde S F, Macdonald J E and Hayden O 2011 *Thin Solid Films* **520** 610–5
[13] Serbena J P M, Machado K D, Siqueira M C, Hümmelgen I A, Mossanek R J O, de Souza G B and da Silva J H D 2014 *J. Phys. D: Appl. Phys.* **47** 015304
[14] Tanioka K, Yamazaki J, Shidara K, Taketoshi K, Kawamura T, Ishioka S and Takasaki Y 1987 *IEEE Electron Dev. Lett.* **8** 392–4
[15] Kasap S O and Rowlands J A 2000 *J. Mater. Sci., Mater. Electron.* **11** 179–98
[16] Kasap S, Frey J B, Belev G, Tousignant O, Mani H, Laperriere L, Reznik A and Rowlands J A 2009 *Phys. Status Solidi* b **246** 1794–805
[17] Wang K, Chen F, Belev G, Kasap S and Karim K S 2009 *Appl. Phys. Lett.* **95** 013505
[18] Lucas P, Conseil C, Yang Z, Hao Q, Cui S, Pledel C B, Bureau B, Gascoin F, Caillaud C, Gulbiten O, Guizouarn T, Baruah P, Li Q and Lucas J 2013 *J. Mater. Chem.* A **1** 8917–25

[19] Kuo T T, Wu C M, Lu H H, Chan I, Wang K and Leou K C 2014 *J. Vac. Sci. Technol.* A **32** 041507
[20] Masuzawa T *et al* 2013 *Sensors* **13** 13744–78
[21] Campbell I H 2011 *Appl. Phys. Lett.* **99** 063303
[22] Siqueira M C, Maia R N A, Araujo R M T, Machado K D, Stolf S F, de Lima J C and Poffo C M 2014 *J. Appl. Phys.* **116** 083514
[23] Kublitski J, Tavares A C B, Serbena J P M, Liu Y, Hu B and Hümmenlgen I A 2016 *J. Solid State Electrochem.* **20** 2191
[24] Siqueira M C, Machado K D, Serbena J P M, Hümmelgen I A, Stolf S F, de Azevedo C G G and da Silva J H D 2016 Electronic and optical properties of amorphous GaSe thin films 2016 *J. Mater. Sci.: Mater. El.* **27** 7379–83
[25] Abrusci A, Stranks S D, Docampo P, Yip H L, Jen A K Y and Snaith H J 2013 *Nano Lett.* **13** 3124−8
[26] Michaelson H B 1977 *J. Appl. Phys.* **48** 4729
[27] Tressa W and Inganäs O 2013 *Sol. Energ. Mater. Sol.* C **117** 599–603
[28] Saive R, Mueller C, Schinke J, Lovrincic R and Kowalsky W 2013 *Appl. Phys. Lett.* **103** 243303
[29] de Castro F A, Heier J, Nuesch F and Hany R 2010 *IEEE J. Sel. Top. Quant.* **16** 1690–9
[30] Gupta D, Bag M and Narayan K S 2008 *Appl. Phys. Lett.* **92** 093301
[31] Hu S, Han P, Wang S, Mao X, Li X and Gao L 2012 *Semicond. Sci. Technol.* **27** 102002
[32] Mao X, Han P, Gao L, Mi Y, Hu S, Fan Y, Zhao C and Wang Q 2011 *IEEE Photonic. Tech. L.* **23** 1517
[33] Gallardo D E, Bertoni C, Dunn S, Gaponik N and Eychmüller A 2007 *Adv. Mater.* **19** 3364–7
[34] Vuuren R D J, Armin A, Pandey A K, Burn P L and Meredith P 2016 *Adv. Mater.* **28** 4766–802
[35] Du L, Luo X, Zhao F, Lv W, Zhang J, Peng Y, Tang Y and Wang Y 2016 *Carbon* **96** 685–94
[36] Reznik A, Baranovskii S D, Rubel O, Jandieri K, Kasap S O, Ohkawa Y, Kubota M, Tanioka K and Rowlands J A 2008 *J. Non-Cryst. Solids* **354** 2691–6
[37] Alavirad M, Roy L and Berini P 2016 *J. Photonics Energ.* **6** 042511
[38] Casalino M, Coppola G, Iodice M, Rendina I and Sirleto L 2012 *Opt. Express* **20** 12599–609
[39] Lao Y F and Perera A G U 2016 *Adv. Opt. Electron.* **2016** 1832097
[40] Griiner J, Remmers M and Neher D 1997 *Adv. Mater.* **9** 964–8
[41] Kumar A, Dey A, Dhir A and Kabra D 2017 *Org. Electron.* **42** 28–33
[42] Choi W *et al* 2012 *Adv. Mater.* **24** 5832–6